# Laser-induced currents along molecular wire junctions

Ignacio Franco, Moshe Shapiro, and Paul Brumer

Citation: The Journal of Chemical Physics **128**, 244906 (2008); doi: 10.1063/1.2940796
View online: http://dx.doi.org/10.1063/1.2940796
View Table of Contents: http://aip.scitation.org/toc/jcp/128/24
Published by the American Institute of Physics



# Laser-induced currents along molecular wire junctions

Ignacio Franco,[1] Moshe Shapiro,[2] and Paul Brumer[1,a)]
[1]*Chemical Physics Theory Group, Department of Chemistry and Center for Quantum Information and Quantum Control, University of Toronto, Toronto, Ontario M5S 3H6, Canada*
[2]*Chemical Physics Department, The Weizmann Institute, Rehovot 76100, Israel and Department of Chemistry and Department of Physics, The University of British Columbia, Vancouver, British Columbia V6T 1Z1, Canada*

(Received 15 January 2008; accepted 16 May 2008; published online 27 June 2008)

The treatment of the previous paper is extended to molecular wires. Specifically, the effect of electron-vibrational interactions on the electronic transport induced by femtosecond $\omega+2\omega$ laser fields along unbiased molecular nanojunctions is investigated. For this, the photoinduced vibronic dynamics of *trans*-polyacetylene oligomers coupled to macroscopic metallic leads is followed in a mean-field mixed quantum-classical approximation. A reduced description of the dynamics is obtained by introducing projective lead-molecule couplings and deriving an effective Schrödinger equation satisfied by the orbitals in the molecular region. Two possible rectification mechanisms are identified and investigated. The first one relies on near-resonance photon-absorption and is shown to be fragile to the ultrafast electronic decoherence processes introduced by the wire's vibrations. The second one employs the dynamic Stark effect and is demonstrated to be highly efficient and robust to electron-vibrational interactions. © *2008 American Institute of Physics*. [DOI: 10.1063/1.2940796]

## I. INTRODUCTION

Considerable effort has been devoted to studies of the properties of molecular wires,[1–7] since they constitute natural candidates for the ongoing miniaturization of electronic devices. Generally, the focus is placed on the transport properties of metal-molecule-metal junctions subject to a bias voltage. In this regime, the metallic leads are the main source of electrons for the transport while the molecular system serves as a transporting medium that can be chemically functionalized to modify the *I-V* characteristics of the junction.

Here, we consider an alternative situation in which the junction is not subject to a bias voltage and where the molecule serves as the main source of transporting electrons. The composite system is taken to be spatially symmetric and net currents are induced using lasers with frequency components $\omega$ and $2\omega$. Such fields give rise to phase-controllable transport in symmetric systems even when they have a zero temporal mean.[8,9] This rectification effect first appears in the third order response of the system to $\omega+2\omega$ fields. At this order, the system mixes the frequencies and harmonics of the incident radiation generating a phase-controllable zero-frequency (dc) component in the response. The setup is of interest since it can produce ultrafast currents and may lead to the development of molecular switches that operate on a femtosecond timescale.

When using $\omega+2\omega$ fields to induce electronic transport, it is crucial to consider the influence of the system's vibrations on the laser scenario. This aspect becomes particularly relevant in molecular wires since molecules nearly always exhibit vibronic couplings that can substantially modify the photophysics of the junction and the effectiveness of the scenario. This characteristic of molecular electronics marks an important difference relative to the behavior of rigid semiconducting solids and is currently the focus of vigorous investigation.[6,10–17]

In this paper, we characterize the influence of vibronic couplings on rectification induced by femtosecond $\omega+2\omega$ laser pulses along unbiased molecular wires. As a system, we consider a *trans*-polyacetylene (PA) oligomer connected by its ends to macroscopic metallic leads. The leads are treated as rigid semi-infinite tight binding chains, and the oligomer is described via the Su-Schrieffer-Heeger (SSH) Hamiltonian.[18,19]

This work is a continuation of our studies in Ref. 20 in which we considered the problem of laser-inducing rectification along isolated PA chains. Naturally, it shares many of the challenges encountered therein. In particular, the problem of how to effectively exert laser control on the electronic dynamics in the presence of lattice-induced decoherence persists. However, it differs significantly from the case of isolated chains since the coupling to the metallic contacts introduces a decay route for energetic electrons and adds an additional element of complexity to the theoretical description.

Besides offering insight into vibrational effects in molecular electronics, this study contributes to the emerging direction of using lasers to modify the transport properties of nanojunctions in which several promising applications are being recognized. For instance, it has been demonstrated that light can induce a switching behavior in the conduction when, upon photoexcitation, the molecule undergoes substantial conformational change.[21–23] In addition, recent theoretical work suggests that lasers may enhance[24,25] or

a)Electronic mail: pbrumer@tikva.chem.utoronto.ca.

 

suppress[26,27] transport induced by a bias or, alternatively, generate currents in unbiased but asymmetric junctions.[26,28,29]

Additional motivation for this study was provided by a rather puzzling observation made in Ref. 30. In that work, the authors analyzed vibrational effects on laser-induced rectification along nanojunctions. The model presented there refers to a two-site molecular wire driven by a continuous wave $\omega+2\omega$ field. In it, each site is coupled perturbatively and independently to one local bath of harmonic oscillators in thermal equilibrium, and an Ohmic spectral density is adopted to describe the phonon-induced relaxation. This work concludes that vibronic couplings *enhance* the current induced by the symmetry breaking field by more than one order of magnitude. This observation seems to be in contradiction with our results in Ref. 20 in which the vibronic couplings were shown to have strong detrimental effects on the control, specially when long pulses are employed. Further, no insight into this rather nonintuitive behavior was provided.

In addition to clarifying this observation, and faithfully characterizing vibrational effects on laser rectification along molecular nanojunctions, a novel mechanism to induce ultrafast currents along molecular wires that relies on the dynamic Stark effect instead of near-resonance photon absorption is discussed here.[31] As shown below, this mechanism is remarkably robust to electron-vibrational couplings and is able to induce large currents in molecular wires with efficiencies $>90\%$.

As in Ref. 20, the photoinduced vibronic dynamics of the wire is followed in a mean-field mixed quantum-classical approximation.[32–35] Electronic decoherence and relaxation is incorporated by averaging over an ensemble of quantum-classical trajectories with initial conditions obtained by importance sampling the ground-state nuclear Wigner phase space distribution. In this manner, the simulations take into account the fact that the vibrational modes in typical molecular wires are nonlocal and constantly kept out of thermal equilibrium either through direct interaction with the field or through exchange of energy with the driven electrons.

A reduced description of the dynamics of the composite system is obtained by deriving an effective Schrödinger equation satisfied by the orbitals in the molecular region. As shown, in the wide bandwidth limit, the lead regions are mapped into negative imaginary (absorbing) potentials. In addition, we employ projective lead-molecule couplings that incorporate basic aspects of the Fermi sea while avoiding the necessity to explicitly follow the dynamics of the essentially infinite number of electrons in the leads. This model is only appropriate to describe the short time dynamics of unbiased junctions since, in it, charge is not permitted to flow from the leads into the oligomer.

This paper is organized as follows. In Sec. II, we briefly describe the model (Sec. II A) and determine the effective mean-field equations of motion for the nanojunction (Sec. II B). Subsequently, we derive an expression for the photoinduced currents (Sec. II C) that solely depends on molecular properties. Our main results are stated in Sec. III. Specifically, in Sec. III A, we study the scenario in its usual regime where the laser frequencies are tuned at or near resonance with one of the electronic transition frequencies. Subsequently, in Sec. III B, we introduce the Stark shift rectification mechanism. The emerging trends are summarized in Sec. IV.

## II. MODEL AND METHODS

### A. Model

As a system, we consider a *trans*-polyacetylene oligomer connected by its ends to macroscopic metallic leads. Since typical metals screen electric fields that have a frequency below the plasma frequency, so that electromagnetic radiation from the optical or the infrared spectral range is almost perfectly reflected at the surface,[36] we assume that the radiation field only interacts with the oligomer chain.

The composite system is described as a one-dimensional lattice in which each site $n$ corresponds to the position of an atom and is defined by the Hamiltonian

$$H(t) = H_L + H_{S\text{-}L} + H_S(t) + H_{S\text{-}R} + H_R. \tag{1}$$

The left ($L$) and right ($R$) leads are treated as semi-infinite rigid tight-binding chains with hopping parameter $t_{\text{lead}}$, so that

$$H_L = -t_{\text{lead}} \sum_{n<0} \sum_{s=\pm 1} (c^\dagger_{n+1,s} c_{n,s} + c^\dagger_{n,s} c_{n+1,s}),$$

$$H_R = -t_{\text{lead}} \sum_{n>N} \sum_{s=\pm 1} (c^\dagger_{n+1,s} c_{n,s} + c^\dagger_{n,s} c_{n+1,s}). \tag{2}$$

Here, $c^\dagger_{n,s}$ ($c_{n,s}$) creates (annihilates) a fermion in site $n$ with spin $s$ and satisfies the usual fermionic anticommutation relations $\{c_{n,s}, c^\dagger_{m,s'}\} = \delta_{n,m}\delta_{s,s'}$. The $N$-membered oligomer chain with Hamiltonian $H_S(t) = H_S^{\text{el}}(t) + H_S^{\text{ph}}(t)$ is situated between sites $n = 1, \ldots, N$ and is described by the SSH model[18,19] coupled to a laser field $E(t)$ in dipole approximation. Specifically, the electronic part of $H_S$ is

$$H_S^{\text{el}}(t) = \sum_{n=1,s}^{N-1} [-t_0 + \alpha(u_{n+1} - u_n)](c^\dagger_{n+1,s} c_{n,s} + c^\dagger_{n,s} c_{n+1,s}) + |e| \sum_{n=1,s}^{N} x_n c^\dagger_{n,s} c_{n,s} E(t), \tag{3}$$

where $t_0$ is the hopping integral for zero displacement, $u_n$ is the monomer displacement of site $n$ from its perfectly periodic position $na$, and $\alpha$ describes the electron-ion coupling between neighboring sites. In turn, $x_n = (na + u_n)$ is the position operator for site $n$, $a$ the lattice constant, and $-|e|$ the unit electronic charge. The lattice is described by

$$H_S^{\text{ph}}(t) = \sum_{n=1}^{N} \frac{p_n^2}{2M} + \frac{K}{2} \sum_{n=1}^{N-1} (u_{n+1} - u_n)^2 - |e| \sum_{n=1}^{N} x_n E(t), \tag{4}$$

with force constant $K$ and (CH) group mass $M$, and where $p_n$ is the momentum conjugate to $u_n$. Lastly, the coupling between the oligomer and the leads

$$H_{S\text{-}L} = -t_{\text{coup}} \sum_{s=\pm 1} (c^\dagger_{1,s} c_{0,s} + c^\dagger_{0,s} c_{1,s})$$

$$H_{S\text{-}R} = -t_{\text{coup}} \sum_{s=\pm 1} (c^{\dagger}_{N+1,s} c_{N,s} + c^{\dagger}_{N,s} c_{N+1,s}), \tag{5}$$

is taken to be at a single site only with coupling constant $t_{\text{coup}}$.

### B. Equations of motion

The electron-vibrational dynamics of the composite system in the presence of a radiation field is followed in the mean-field (Ehrenfest) mixed quantum-classical approximation introduced in Sec. II B of Ref. 20. As before, the nuclei satisfy classical trajectories governed by

$$\dot{u}_n(t) = \frac{p_n(t)}{M},$$

$$\dot{p}_n(t) = -K(2u_n(t) - u_{n+1}(t) - u_{n-1}(t)) + 2\alpha\, \text{Re}\{\rho_{n,n+1}(t) - \rho_{n,n-1}(t)\} - |e|E(t)(\rho_{n,n}(t) - 1), \tag{6}$$

where $\rho_{n,m}(t) = \Sigma_s \langle \Psi(t)| c^{\dagger}_{n,s} c_{m,s} |\Psi(t)\rangle$ is the reduced electronic density matrix. The chain is taken to be clamped so that $u_1(t) = u_N(t) = 0$ and $p_1(t) = p_N(t) = 0$, and Eq. (6) is valid for $n = 2, \ldots, N-1$. In turn, the many electron wavefunction $|\Psi(t)\rangle$ satisfies the Schrödinger equation and, hence, the dynamics of $\rho_{n,m}(t)$ is given by

$$i\hbar \frac{d}{dt} \rho_{n,m}(t) = \sum_s \langle \Psi(t)| [c^{\dagger}_{n,s} c_{m,s}, H_{\text{elec}}(t)] |\Psi(t)\rangle, \tag{7}$$

where

$$H_{\text{elec}}(t) = H_L + H_{S\text{-}L} + H^{\text{el}}_S(t) + H_{S\text{-}R} + H_R \tag{8}$$

is the electronic part of the Hamiltonian. For an initial electronic state $|\Psi(0)\rangle$ that is well described by a single Slater determinant, the reduced density matrix admits the orbital decomposition

$$\rho_{n,m}(t) = \sum_{\epsilon,s} \langle \epsilon(t), s| n, s\rangle \langle m, s| \epsilon(t), s\rangle f(\epsilon, s), \tag{9}$$

where $f(\epsilon, s)$ is the time-independent initial distribution function that takes values 0 or 1 depending on the occupation of each level with energy $\epsilon$ and spin $s$, and $|n, s\rangle = c^{\dagger}_{n,s}|0\rangle$, where $|0\rangle$ represents the vacuum state. In order for $\rho_{n,m}(t)$ to satisfy Eq. (7), the orbitals $|\epsilon(t), s\rangle$ must be solutions to the single-particle time-dependent Schrödinger equation

$$i\hbar \frac{d}{dt} |\epsilon(t), s\rangle = H_{\text{elec}}(t) |\epsilon(t), s\rangle \tag{10}$$

with initial condition $|\epsilon(t=0), s\rangle = |\epsilon, s\rangle$, where $|\epsilon, s\rangle$ denote the eigenorbitals of $H_{\text{elec}}$ at preparation time.

In principle, by integrating the above equations self-consistently, it is possible to follow the coupled dynamics of both electronic and nuclear degrees of freedom in the composite system. In practice, the problem is intractable since the number of equations to be integrated is unbounded due to the large number of electrons in the leads and the spatial unboundedness of the composite system. Further, the simplifications that have been developed for periodic systems are not applicable here. A reduced description of the dynamics is obtained by first deriving, in Sec. II B 1, an effective single-particle Schrödinger equation that is satisfied in the molecular region. This eliminates the necessity of integrating Eq. (10) over the complete spatial domain of the composite system. Subsequently, in Sec. II B 2, we specialize the coupling between the molecule and the leads using projection operators so that basic aspects of the lead-molecule coupling are captured without explicitly following the dynamics of the electrons originally in the leads. Then, in Sec. II B 3, we derive an expression for the memory kernel of the resulting equations, which is then employed in Sec. II B 4 to obtain the Markovian limit of the dynamics.

#### 1. Effective non-Markovian Schrödinger equation

Henceforth, we drop spin labels since orbitals with the same energy but opposite spin satisfy the same equation of motion under $H_{\text{elec}}(t)$. We begin by partitioning the orbitals that form $\rho_{n,m}(t)$ into the three spatial regions of the composite system

$$|\epsilon(t)\rangle = |\epsilon_L(t)\rangle + |\epsilon_S(t)\rangle + |\epsilon_R(t)\rangle. \tag{11}$$

Here, $|\epsilon_P(t)\rangle = \Sigma_{n \in P} \langle n|\epsilon(t)\rangle |n\rangle$ describes the part of the orbital in region $P$, where $P$ can be the left lead ($L$), right lead ($R$), or system ($S$). In terms of this partition, the single-particle Schrodinger Eq. (10) reads

$$i\hbar \frac{d}{dt} \begin{bmatrix} |\epsilon_L(t)\rangle \\ |\epsilon_S(t)\rangle \\ |\epsilon_R(t)\rangle \end{bmatrix} = \begin{bmatrix} H_L & H_{S\text{-}L}(t) & 0 \\ H_{S\text{-}L}(t) & H^{\text{el}}_S(t) & H_{S\text{-}R}(t) \\ 0 & H_{S\text{-}R}(t) & H_R \end{bmatrix} \begin{bmatrix} |\epsilon_L(t)\rangle \\ |\epsilon_S(t)\rangle \\ |\epsilon_R(t)\rangle \end{bmatrix}, \tag{12}$$

where we have explicitly allowed for time dependence in the lead-molecule coupling since this characteristic will arise when introducing projection operators into the dynamics.

We seek an effective equation of motion for $|\epsilon_S\rangle$ in which it is not necessary to explicitly follow the dynamics of $|\epsilon_L\rangle$ or $|\epsilon_R\rangle$.[37] This can be accomplished by Laplace transforming the evolution equation for the lead components, solving the resulting algebraic equations and inverse Laplace transforming by taking into account the convolution theorem. The procedure yields

$$|\epsilon_\beta(t)\rangle = U^{\beta}(t) |\epsilon_\beta(0)\rangle + \frac{1}{i\hbar} \int_0^t U^{\beta}(t-\tau) H_{S-\beta}(\tau) |\epsilon_S(\tau)\rangle d\tau, \tag{13}$$

where $\beta = L$ or $R$ denotes the left or right lead, respectively. The first term in Eq. (13) describes the evolution of the lead components of the orbitals in the absence of coupling to the molecular system. Naturally, the dynamics is determined by the evolution operator for the isolated leads $U^{\beta}(t) = \exp(-iH_\beta t/\hbar)$. In turn, the influence of the lead-molecule coupling is mapped into a convolution integral with $U^{\beta}(t-\tau)$ acting as the memory kernel.

By introducing Eq. (13) into the evolution equation for $|\epsilon_S\rangle$, we arrive at an effective non-Markovian Schrödinger equation for the system part of the orbital:

$$i\hbar\frac{d}{dt}|\epsilon_S(t)\rangle = H_S(t)|\epsilon_S(t)\rangle + \sum_{\beta=L,R}\left[H_{S-\beta}(t)U^{\beta}(t)|\epsilon_\beta(0)\rangle + \frac{H_{S-\beta}(t)}{i\hbar}\int_0^t U^{\beta}(t-\tau)H_{S-\beta}(\tau)|\epsilon_S(\tau)\rangle d\tau\right]. \quad (14)$$

The first term corresponds to the single-particle Schrödinger equation for the isolated system. The remaining terms describe the transfer of population amplitude between the system and the leads.

The advantage of Eq. (14) over Eq. (10) is that it permits following the dynamics of the composite system by integrating the equations of motion in a finite spatial region. The influence of the leads has been mapped into a term that is nonlocal in time and a residual term dependent on the initial state of the leads. Equation (14) is also a good starting point for various approximations. In particular, the Markovian limit arises naturally when the energy bandwidth of the metallic leads is much larger than any other characteristic energy of the system.

### 2. Projective molecule-lead coupling

Solving the above integro-differential equation [Eq. (14)] exactly for all the initially occupied levels in the composite system is a problem as formidable as the original one, and an effective way to introduce the leads into the dynamics is required. Physically, the contacts block any electrons from the molecule with energy less than the Fermi energy and act as a thermal source of electrons to the molecular system. We are interested in the case where there is no bias voltage across the bridge and in short simulation times that limit the degree of relaxation of electrons from the leads to the molecular states. In this regime, the main effect of the leads is to accept electrons that have energy higher than the Fermi energy $\epsilon_F$ and to block them otherwise. We model this property using projection operators that restrict the interaction between the molecule and the leads to only those molecular levels that are above the Fermi energy.

Consider a projection operator ($\mathcal{P}^2=\mathcal{P}$)

$$\mathcal{P}(t) = \mathcal{P}^S(t) + \mathcal{P}^L + \mathcal{P}^R, \quad (15)$$

where

$$\mathcal{P}^\beta = \sum_{\epsilon\in\beta}|\epsilon_\beta\rangle\langle\epsilon_\beta|, \quad (16)$$

with $\beta=L$ or $R$, projects onto single-particle states of the left/right lead. In turn,

$$\mathcal{P}^S(t) = \sum_{\epsilon_\gamma>\epsilon_F}|\gamma_S(t)\rangle\langle\gamma_S(t)| \quad (17)$$

is a projection operator onto the instantaneous light-dressed eigenorbitals $|\gamma_S(t)\rangle$ of the molecular system that reside above the Fermi energy. The latter are defined by the eigenvalue relation

$$H_S^{\mathrm{el}}(t)|\gamma_S(t)\rangle = \epsilon_\gamma(t)|\gamma_S(t)\rangle, \quad (18)$$

where $H_S^{\mathrm{el}}(t)$ is the electronic Hamiltonian of the oligomer at time $t$ given in Eq. (3). The time-dependence of $|\gamma_S(t)\rangle$ [and $\mathcal{P}^S(t)$] is a result of the time dependence in the electronic Hamiltonian introduced by the field and the nuclear motion. An evident but important property of the projection operator is that $\mathcal{P}^S\mathcal{P}^\beta=\mathcal{P}^\beta\mathcal{P}^S=0$.

We now wish to use $\mathcal{P}$ to restrict the lead-molecule interaction. The projection operator cannot be introduced directly into the second quantized version of the lead-molecule coupling [Eq. (5)]. Rather, it is necessary to modify the first-quantized interaction Hamiltonian and then second quantize it. In first quantization, the original coupling takes the form $H_{S-\beta}=\Sigma_{i=1}^{\mathcal{N}}h_{S-\beta}(i)$, where the label $i$ refers to the coordinates of the $i$th electron and the sum runs over all $\mathcal{N}$ electrons in the system. The nearest-neighbor couplings of Eq. (5) give rise to the following matrix elements of $h_{S-\beta}$:

$$\langle n|h_{S-L}|m\rangle = -t_{\mathrm{coup}}(\delta_{n,1}\delta_{m,0}+\delta_{n,0}\delta_{m,1}),$$

$$\langle n|h_{S-R}|m\rangle = -t_{\mathrm{coup}}(\delta_{n,N}\delta_{m,N+1}+\delta_{n,N+1}\delta_{m,N}). \quad (19)$$

By introducing $\mathcal{P}$ into the first-quantized coupling Hamiltonian, so that

$$H_{S-\beta}(t) = \sum_{i=1}^{\mathcal{N}}\mathcal{P}^\dagger(i,t)h_{S-\beta}(i)\mathcal{P}(i,t), \quad (20)$$

only those electrons in the desired subset of electronic levels are allowed to move from the molecule to the leads, and vice versa. The modified coupling operator is Hermitian, and thus diagonalizable, and hence can be cast into second-quantized form using the usual procedure,[38] to obtain

$$H_{S-L}(t) = -t_{\mathrm{coup}}\sum_{n,m,s}\mathcal{P}_{n,0}(t)\mathcal{P}_{1,m}(t)c_{n,s}^\dagger c_{m,s} + \mathrm{H.c.},$$

$$H_{S-R}(t) = -t_{\mathrm{coup}}\sum_{n,m,s}\mathcal{P}_{n,N}(t)\mathcal{P}_{N+1,m}(t)c_{n,s}^\dagger c_{m,s} + \mathrm{H.c.}, \quad (21)$$

where $\mathcal{P}_{n,m}=\langle n|\mathcal{P}|m\rangle$ and H.c. stands for Hermitian conjugate.

We specialize our considerations to the case in which electrons in the molecule are allowed to leak into the leads but where no electrons that are originally in the leads can enter the molecule. This is modeled by treating the leads as electronless and by coupling the excited electrons in the molecular system to every level in the leads. Since we now project onto a complete lead basis, $\mathcal{P}_{n,0}=\delta_{n,0}$ and $\mathcal{P}_{n,N+1}=\delta_{n,N+1}$, and the lead-molecule interaction terms assume the simplified form:

$$H_{S-L}(t) = -t_{\mathrm{coup}}\sum_{n\in S}\sum_{s=\pm1}\mathcal{P}_{1,n}^S(t)c_{0,s}^\dagger c_{n,s} + \mathrm{H.c.},$$

$$H_{S-R}(t) = -t_{\mathrm{coup}}\sum_{n\in S}\sum_{s=\pm1}\mathcal{P}_{N,n}^S(t)c_{N+1,s}^\dagger c_{n,s} + \mathrm{H.c.} \quad (22)$$

The leads and molecule are taken to be initially detached and, since the projective coupling [Eq. (22)] already incorporates the Fermi blockade imposed by the leads, we only consider orbitals that are initially in the molecular region so

that $|\epsilon_\beta(t=0)\rangle=0$ for the states of interest. Taking into account the above, and introducing the projective coupling (22) into Eq. (14), it follows that

$$i\hbar\frac{d}{dt}\langle n|\epsilon_S(t)\rangle=\sum_{m=1}^{N}\langle n|H_S^{\mathrm{el}}(t)|m\rangle\langle m|\epsilon_S(t)\rangle + \frac{t_{\mathrm{coup}}^2}{i\hbar}\sum_{m=1}^{N}\int_0^t[\mathcal{P}_{n,1}^S(t)U_{0,0}^L(t-\tau)\mathcal{P}_{1,m}^S(\tau) + \mathcal{P}_{n,N}^S(t)U_{N+1,N+1}^R(t-\tau)\mathcal{P}_{N,m}^S(\tau)] \times\langle m|\epsilon_S(\tau)\rangle d\tau. \tag{23}$$

### 3. The memory kernel

To proceed further, an explicit expression for the memory kernels in Eq. (23) is required. The task is to find the matrix elements of the evolution operator $U^\beta(t)=\exp(-iH_\beta t/\hbar)$ for the left ($\beta=L$) and right ($\beta=R$) semi-infinite tight binding chains in site representation. For this, first note that the lead Hamiltonian [Eq. (2)] can be diagonalized by performing the basis transformation:

$$c_{n,s}=\left(\frac{2}{\Omega}\right)^{1/2}\sum_{k=1}^{\Omega}\sin[(n-n_\beta)k\pi/\Omega]c_{k,s}, \tag{24}$$

where $\Omega$ is the number of sites in the leads and $n_\beta$ is the molecular site that is connected to lead $\beta$, i.e., $n_L=1$ and $n_R=N$. Inserting Eq. (24) into Eq. (2) yields

$$H_\beta=-2t_{\mathrm{lead}}\sum_{k=1}^{\Omega}\sum_{s=\pm1}\cos(k\pi/\Omega)c_{k,s}^\dagger c_{k,s} \tag{25}$$

where we have exploited the fact that for large $\Omega$, $\delta_{k,k'}=(1/\Omega)\Sigma_{n=1}^{\Omega-1}\exp(in(k-k')\pi/\Omega)$.

The matrix elements of the evolution operator in site representation $n$ are then given by

$$U_{n,m}^\beta(t)=\langle n|U^\beta(t)|m\rangle = \frac{2}{\Omega}\sum_{k=1}^{\Omega}\sin[(n-n_\beta)k\pi/\Omega] \times\sin[(m-n_\beta)k\pi/\Omega]\exp[2it_{\mathrm{lead}}\cos(k\pi/\Omega)t/\hbar],$$

where we have used Eqs. (24) and (25). For large $\Omega$, the sum can be approximated by an integral to give

$$U_{n,m}^\beta(t)=-\frac{1}{\pi}\int_0^\pi\{\cos[(n+m-2n_\beta)\theta] - \cos[(n-m)\theta]\}\exp[2it_{\mathrm{lead}}\cos(\theta)t/\hbar]d\theta = i^{n-m}J_{n-m}\left(\frac{2t_{\mathrm{lead}}}{\hbar}t\right)-i^{n+m-2n_\beta}J_{n+m-2n_\beta}\left(\frac{2t_{\mathrm{lead}}}{\hbar}t\right), \tag{26}$$

where $J_n(z)=(i^{-n}/\pi)\int_0^\pi e^{iz\cos\theta}\cos(n\theta)d\theta$ is a Bessel function of the first kind of order $n$.[39] We note that $U_{n,m}^\beta$ satisfies the equations of motion, as well as the boundary and initial conditions:

$$i\hbar\frac{d}{dt}U_{n,m}^\beta(t)=\sum_{r\in\beta}\langle n|H_\beta|r\rangle U_{r,m}^\beta(t),$$

$$U_{n_\beta,m}^\beta(t)=U_{m,n_\beta}^\beta(t)=0,$$

$$U_{n,m}^\beta(t=0)=\delta_{n,m}.$$

Of particular relevance is

$$\mathcal{K}(t)\equiv U_{0,0}^L(t)=U_{N+1,N+1}^R(t)=\frac{2J_1((2t_{\mathrm{lead}}/\hbar)t)}{(2t_{\mathrm{lead}}/\hbar)t}, \tag{27}$$

where we have used the identities $J_{-n}(z)=(-1)^nJ_n(z)$ and $J_{n-1}(z)+J_{n+1}(z)=(2n/z)J_n(z)$. This quantity determines the kernel of the convolution integral in Eq. (23). It is characterized by a pronounced peak around $t=0$ followed by oscillations that decay asymptotically as $(1/\sqrt{\pi})(\hbar/t_{\mathrm{lead}}t)^{3/2}$. This asymptotic dependence is exploited in the next section to derive the Markovian limit of the equations of motion.

### 4. Wide bandwidth approximation

We now invoke the wide bandwidth approximation in which the energy bandwidth of the leads ($4t_{\mathrm{lead}}$) becomes the dominant energy in the problem and, consequently, $\hbar/t_{\mathrm{lead}}$ the fastest time scale. In this regime, the memory kernel $\mathcal{K}(t-\tau)$ becomes sharply peaked around $\tau=t$ and the orbitals do not change appreciably on the time scale in which $\mathcal{K}(t-\tau)$ varies. It follows that the convolution integrals in Eq. (23) can be approximated by

$$\int_0^t\mathcal{P}_{n,k}^S(t)\mathcal{K}(t-\tau)\mathcal{P}_{k,m}^S(\tau)\langle m|\epsilon_S(\tau)\rangle d\tau \approx\mathcal{P}_{n,k}^S(t)\mathcal{P}_{k,m}^S(t)\langle m|\epsilon_S(t)\rangle\int_0^t\mathcal{K}(t-\tau)d\tau.$$

Further, for times $t\gg\hbar/t_{\mathrm{lead}}$, the remaining time integral is well approximated by its asymptotic value,

$$\lim_{t\to\infty}\int_0^t\mathcal{K}(t-\tau)d\tau=\hbar/t_{\mathrm{lead}},$$

and the equations of motion reduce to their Markovian limit:

$$i\hbar\frac{d}{dt}\langle n|\epsilon_S(t)\rangle=\sum_{m=1}^{N}\left[\langle n|H_S^{\mathrm{el}}(t)|m\rangle-i\frac{t_{\mathrm{coup}}^2}{t_{\mathrm{lead}}}\Gamma_{n,m}(t)\right]\langle m|\epsilon_S(t)\rangle, \tag{28}$$

where

$$\Gamma_{n,m}(t)=\mathcal{P}_{n,1}^S(t)\mathcal{P}_{1,m}^S(t)+\mathcal{P}_{n,N}^S(t)\mathcal{P}_{N,m}^S(t). \tag{29}$$

Equation (28) provides a realistic mechanism for electron absorption and energy dissipation in the dynamics of a metal-molecule-metal system. The influence of the leads in the dynamics has been mapped into a negative imaginary (absorbing) potential. The projection operators in the coupling, contained within $\Gamma_{n,m}$, ensure that only those electrons with sufficient energy get absorbed, with proper conservation of the antisymmetry principle of the many-electron wavefunction. The equation is valid for times $t\gg\hbar/t_{\mathrm{lead}}$ but can be applied for all times by turning on slowly the interaction between the molecule and the leads, a strategy that we adopt.

Note that the field influences the dynamics directly by modifying the wire component and indirectly by influencing the wire-lead coupling since $\Gamma_{n,m}(t)$ depends both on the nuclear dynamics and the radiation-matter interaction. This characteristic introduced by the field has also been observed in an alternative description of the laser-induced dynamics of molecular wires.[27] Further note that this model neglects hole transport. Nevertheless, since the SSH Hamiltonian is electron-hole symmetric, a subsequent inclusion of this contribution is just expected to double the resulting current.

#### 5. Final equations

Consider now the final equations of motion. The nuclear degrees of freedom satisfy trajectories determined by Eq. (6). The orbitals determining $\rho_{n,m}(t)$ [Eq. (9)] are the initially occupied molecular orbitals which, by virtue of Eq. (28), satisfy

$$\begin{aligned} i\hbar\frac{d}{dt}\langle n|\epsilon_S(t)\rangle &= [-t_0+\alpha(u_{n+1}(t)-u_n(t))]\langle n+1|\epsilon_S(t)\rangle \\ &+[-t_0+\alpha(u_n(t)-u_{n-1}(t))]\langle n-1|\epsilon_S(t)\rangle \\ &+|e|E(t)(na+u_n(t))\langle n|\epsilon_S(t)\rangle \\ &-i\frac{t_{\mathrm{coup}}^2}{t_{\mathrm{lead}}}\sum_{m=1}^{N}\Gamma_{n,m}(t)\langle n|\epsilon_S(t)\rangle, \end{aligned} \tag{30}$$

for $n=2,\ldots,N-1$. At the boundaries of the oligomer, $n=1$ and $n=N$, the orbitals satisfy Eq. (30) without the term that involves the amplitude of the orbital amplitudes outside the molecular domain. Equations (6) and (30), together with the auxiliary quantity (9), constitute a closed set of $N(N+2)$ coupled first-order differential equations that are integrated using a Runge-Kutta method of order 8.[40] The projective term in the dynamics $\Gamma_{n,m}(t)$ is updated at every time step by diagonalizing the system's electronic Hamiltonian $H_S^{\mathrm{el}}(t)$ to obtain the instantaneous eigenstates $|\gamma_S(t)\rangle$ defining the projection operator through Eq. (17). We project onto states that are above the Fermi energy, taken to be the zero reference energy. In other words, out of the $N$ single-particle instantaneous eigenstates of $H_S^{\mathrm{elec}}(t)$, we project onto the upper $N/2$ states. The metal-molecule coupling is turned on smoothly and slowly (in 10 fs) from preparation time.

Electronic dephasing due to vibronic couplings is incorporated by integrating the above equations of motion for an ensemble of initial conditions. The initial conditions are generated using the strategy detailed in Sec. II C of Ref. 20. Briefly, the starting optimal geometry of the oligomer is obtained by minimizing the total ground-state energy of the chain. Then, a normal mode analysis around this geometry is performed, yielding the ground state nuclear Wigner phase space distribution function in the harmonic approximation. By importance sampling this distribution, an ensemble of lattice initial conditions $\{\boldsymbol{u}^i(0),\boldsymbol{p}^i(0)\}$ is generated. The associated initial values for the orbitals $\{|\boldsymbol{\epsilon}^i(0)\rangle\}$ are obtained by diagonalizing the electronic part of the Hamiltonian for each initial nuclear geometry $\{\boldsymbol{u}^i(0)\}$. Each member $i$ of the ensemble defines a quantum-classical trajectory and the set is used to obtain ensemble averages.

Throughout this work, we use the standard SSH parameters for PA:[19] $\alpha=4.1$ eV/Å, $K=21$ eV/Å$^2$, $t_0=2.5$ eV, $M=1349.14$ eV fs$^2$/Å$^2$, and $a=1.22$ Å. In turn, we take the molecule and leads to be weakly coupled with $t_{\mathrm{coup}}^2/t_{\mathrm{lead}}=0.1$ eV.

### C. Dynamical observables

The vibronic dynamics is characterized by the geometric and spectroscopic properties defined in Sec. II D of Ref. 20. In addition, an expression for the current that depends solely on molecular properties is required and is obtained in this section.

The current entering into lead $\beta=L,R$ is defined by

$$j_\beta=-|e|\frac{\partial p_\beta}{\partial t}, \tag{31}$$

where $p_\beta$ is the number of electrons in lead $\beta$. In terms of the reduced density matrix, $j_\beta$ can be expressed as

$$j_\beta=-|e|\sum_{n\in\beta}\frac{\partial\rho_{n,n}}{\partial t}=\frac{i}{\hbar}|e|\sum_{n\in\beta,s}\langle\Psi(t)|[c_{n,s}^\dagger c_{n,s},H_{\mathrm{elec}}]|\Psi(t)\rangle, \tag{32}$$

where we have used Eq. (7). For the Hamiltonian in Eq. (8), only the commutator with the lead-molecule coupling contributes to the current,

$$j_\beta=\frac{i}{\hbar}|e|\sum_{n\in\beta,s}\langle\Psi(t)|[c_{n,s}^\dagger c_{n,s},H_{S-\beta}]|\Psi(t)\rangle. \tag{33}$$

Introducing the projective coupling [Eq. (22)] into the above expression, we have that

$$\begin{aligned} j_L&=\frac{2|e|t_{\mathrm{coup}}}{\hbar}\sum_{m\in S}\mathrm{Im}\{\mathcal{P}_{1,m}^S(t)\rho_{0,m}(t)\}, \\ j_R&=\frac{2|e|t_{\mathrm{coup}}}{\hbar}\sum_{m\in S}\mathrm{Im}\{\mathcal{P}_{N,m}^S(t)\rho_{N+1,m}(t)\}. \end{aligned} \tag{34}$$

Equation (34) indicates that the current entering into the leads depends on the spatial coherences between the lead boundary and every site in the molecular system. We desire, however, an expression that solely depends on molecular properties. For this, we exploit Eq. (13) in its Markovian limit according to which

$$\begin{aligned} \langle 0|\epsilon(t)\rangle&=i\frac{t_{\mathrm{coup}}}{t_{\mathrm{lead}}}\sum_m\mathcal{P}_{1,m}^S(t)\langle m|\epsilon_S(t)\rangle, \\ \langle N+1|\epsilon(t)\rangle&=i\frac{t_{\mathrm{coup}}}{t_{\mathrm{lead}}}\sum_m\mathcal{P}_{N,m}^S(t)\langle m|\epsilon_S(t)\rangle, \end{aligned} \tag{35}$$

so that

$$\rho_{0,m}(t)=-i\frac{t_{\mathrm{coup}}}{t_{\mathrm{lead}}}\sum_n\mathcal{P}_{n,1}^S(t)\rho_{n,m}(t),$$

TABLE I. Parameters and labels defining the femtosecond laser pulses used $E(t)=\exp(-(t-T_c)^2/T_W^2)(\epsilon_\omega\cos(\omega t+\phi_\omega)+\epsilon_{2\omega}\cos(2\omega t+\phi_{2\omega}))$. Here, $I_{2\omega}$ is the intensity of the $2\omega$ component at maximum field strength.

| Label | $T_c$(fs) | $T_W$(fs) | $\epsilon_{2\omega}$ (V Å$^{-1}$) | $\epsilon_\omega/\epsilon_{2\omega}$ | $I_{2\omega}$ (W cm$^{-2}$) |
|---|---|---|---|---|---|
| f1 | 900 | 300 | $8.70\times10^{-3}$ | 2.82 | $1.0\times10^{9}$ |
| f2 | 900 | 300 | $4.00\times10^{-2}$ | 2.82 | $2.1\times10^{10}$ |
| f3 | 50 | 10 | $8.70\times10^{-3}$ | 2.82 | $1.0\times10^{9}$ |
| f4 | 50 | 10 | $4.00\times10^{-2}$ | 2.82 | $2.1\times10^{10}$ |

$$\rho_{N+1,m}(t)=-i\frac{t_{\text{coup}}}{t_{\text{lead}}}\sum_n \mathcal{P}^S_{n,N}(t)\rho_{n,m}(t). \tag{36}$$

Substituting Eq. (36) into Eq. (34) gives an expression for the current that is completely defined by molecular properties,

$$j_\beta(t)=-\frac{2|e|}{\hbar}\frac{t_{\text{coup}}^2}{t_{\text{lead}}}\sum_{m,n}\text{Re}\{\mathcal{P}^S_{n_\beta,m}(t)\mathcal{P}^S_{n,n_\beta}(t)\rho_{n,m}(t)\}, \tag{37}$$

as desired. Another useful quantity is the amount of charge that has been deposited in lead $\beta$ at a given time. This is defined by

$$q_\beta(t)=\int_0^t j_\beta(\tau)d\tau. \tag{38}$$

Any rectification generated by an $\omega+2\omega$ pulse results in $q_L-q_R\neq0$.

## III. RESULTS AND DISCUSSION

In Ref. 20, important ways in which the electron-vibrational couplings influence the photoinduced dynamics of isolated PA chains were identified. The coupling introduces a significant exchange of energy between vibrational and electronic degrees of freedom, broadening of the electronic transitions, pronounced changes in the mean single particle spectrum during and after the laser pulse, internal relaxation mechanisms, and ultrafast decoherence (in less than 10 fs). By contrast, in rigid systems, no energy is transferred between the electronic and nuclear degrees of freedom, and changes in the electronic spectrum are only due to Stark shifts induced by the laser field.

Here, we analyze the extent in which the vibronic couplings affect the ability of $\omega+2\omega$ lasers to induce currents along molecular wires. Vibrational effects are made evident by contrasting the ensemble-averaged electron-vibrational evolution of the bridge with the dynamics of a single rigid trajectory that stays frozen at the optimal geometry. The wire is made rigid by arbitrarily increasing the mass of the (CH) groups by $10^6$. In this way, the electron-ion interaction remains constant but the lattice moves a thousand times slower. Two different regimes of operation are considered. In Sec. III A, the scenario is applied in its usual form where the field frequencies are tuned at or near an electronic resonance and electrons are promoted to the excited states through near-resonance photon absorption. In Sec. III B, a novel mechanism is introduced in which the field is kept far off resonance and excitation is done through the dynamic Stark effect. As shown below, in the presence of vibrations, the first scenario becomes inefficient while the Stark shift scenario remains robust.

### A. Currents through near-resonance excitation

We investigate the dynamics and currents onset by the laser pulses specified in Table I for different laser frequencies and relative phases noted in the text. The parameters chosen for the pulses are meant to encompass four illustrative cases: dynamics induced by weak and moderately strong pulses with time envelopes that are either comparable (10 fs) or long (300 fs) compared to the typical electronic dephasing time. The laser frequencies are chosen to be at or near resonance so that, in this case, near-resonance photon absorption is the main source of electronic excitation.

The system consists of neutral PA wires composed of 20 sites and 20 $\pi$ electrons ($L\approx23$ Å) initially in the ground electron-vibrational state. An ensemble of 40 000 initial configurations is propagated. This oligomer size was selected because it is representative of molecules that have been employed in constructing molecular nanojunctions.[5] The initial geometry of the chain consists of a perfect alternation of double and single bonds. The electronic structure is composed of 20 doubly occupied valence $\pi$ orbitals and 20 empty $\pi^\star$ states, separated by an energy gap of $2\Delta=1.8$ eV. A detailed account of the initial configuration is provided in Ref. 20.

We begin by presenting two concrete examples of the currents induced on flexible and rigid PA wires by $\omega+2\omega$ pulses. Figures 1 and 2 show the charge deposited in the left and right leads during and after photoexcitation with a moderately strong 10 fs pulse (field f4 in Table I) and a weak

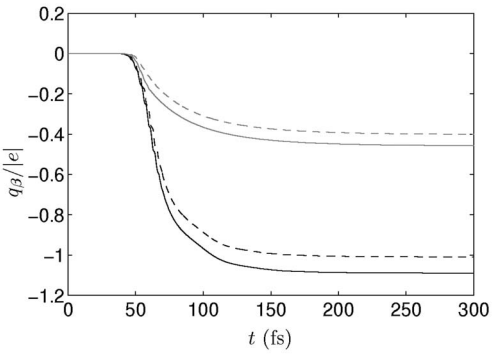


FIG. 1. Charge deposited in the left (solid lines) and right (broken lines) contacts during and after photoexcitation with pulse f4. Here, $\hbar\omega=1.3$ eV, $\phi_{2\omega}-2\phi_\omega=0$ (black lines, flexible wire; gray lines, rigid case).

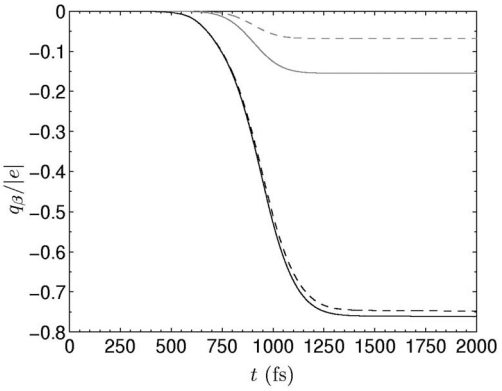


FIG. 2. Total charge entering the left (solid lines) and right (broken lines) leads during and after photoexcitation with pulse f1 with $\hbar\omega$=1.2 eV, $\phi_{2\omega}-2\phi_\omega=0$ (gray lines, rigid wire; black line, flexible case).

300 fs pulse (field f1) resonantly coupling valence and conduction bands, respectively. Here, $\phi_{2\omega}-\phi_\omega=0$. As can be seen, symmetry breaking is achieved while the system is being driven by the laser field. After the pulse, any remaining electrons with energy higher than the Fermi energy are absorbed symmetrically by the left and right contacts. At the particular frequency chosen, we observe that the degree of symmetry breaking induced by the 10 fs pulse in the rigid and flexible chain is of the same order of magnitude. Note, however, that in the flexible wire considerably more electrons are excited across the energy gap than in the rigid example, due to the level broadening introduced by the wire's vibrations. Most of these electrons do not contribute to the rectification. As discussed below, this is a recurrent motif when applying the near-resonance $\omega+2\omega$ scenario to flexible systems. In the case of photoexcitation with a 300 fs pulse, and for the parameters chosen in Fig. 2, in rigid wires most of the photoexcited electrons participate in forming the dc current. In flexible wires, however, most excited electrons do not contribute to the net current. Although individual trajectories may exhibit large rectification effects, there is almost a perfect cancellation when the individual contributions are added together. The decoherence is simply too fast to allow maintenance of the rectification effect.

We now focus on the net asymptotic current induced by all of the laser pulses of Table I, for different laser frequencies. The quantities of interest are the net difference in charge deposited in the left and right leads $q_L-q_R$, and the overall efficiency of the process $\eta=(q_L-q_R)/(q_L+q_R)$, where $q_\beta$ is the total charge deposited at lead $\beta$. Ideally, one would like to find driving parameters that induce sizable currents in the nanojunction with high efficiency.

Figures 3 and 4 show $q_L-q_R$ and $\eta$ after excitation with pulses f1–f4 for different laser frequencies, with $\phi_{2\omega}-2\phi_\omega=0$. Consider first the rigid chain results. For rigid chains, the degree of control and the net induced currents are considerable. The effect is enhanced by tuning the frequency components of the laser near one of the system's electronic transition frequencies. At selected frequencies, the process can achieve efficiencies as high as ~60%. Note, however, that for exact on-resonance driving frequencies, the efficiencies are low due to competing multiphoton processes that populate the excited states but do not contribute to the currents. By applying stronger pulses [Fig. 3(b)], it is possible to exploit higher order multiphoton processes to induce rectification, resulting in a complicated frequency dependence to the control map. When short pulses are employed [Figs. 3(c) and 3(d)], the sharp features observed in the long-pulse control are no longer resolved. For rigid wires, higher efficiencies are achieved by using long weak pulses at frequencies that minimize satellite photoexcitations. When employing either short or very strong pulses, satellite absorptions, arising from either competing multiphoton processes or parasite absorption at frequencies contained within the bandwidth of the pulse, are unavoidable.

The inclusion of vibrations in the dynamics substantially

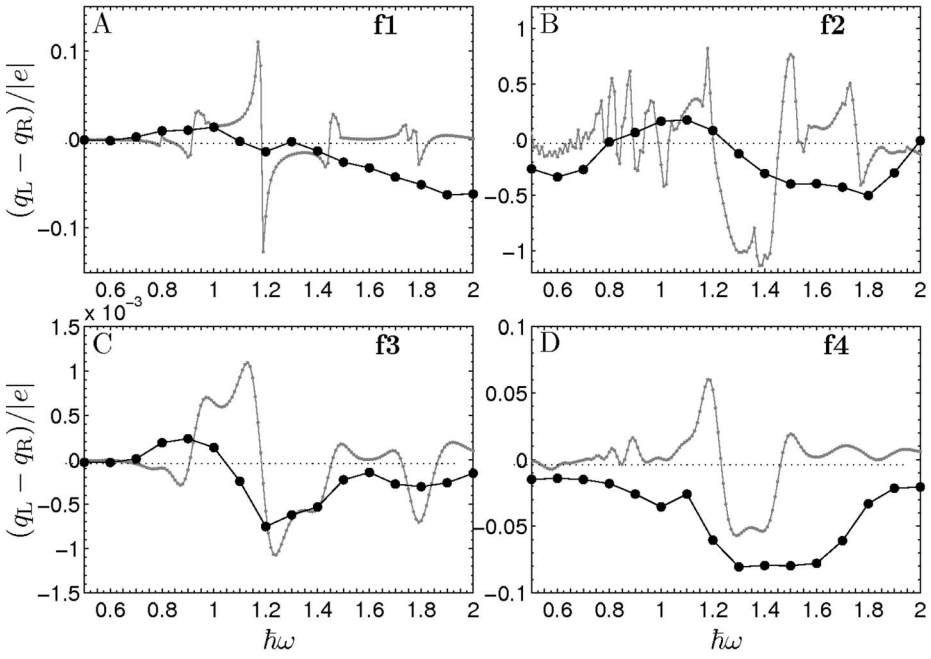


FIG. 3. Frequency dependence of the net difference in charge deposited by pulse: (A) f1, (B) f2, (C) f3, and (D) f4, with $\phi_{2\omega}-2\phi_\omega=0$. The black dots show the behavior of the flexible chain, while the gray lines correspond to the rigid case.

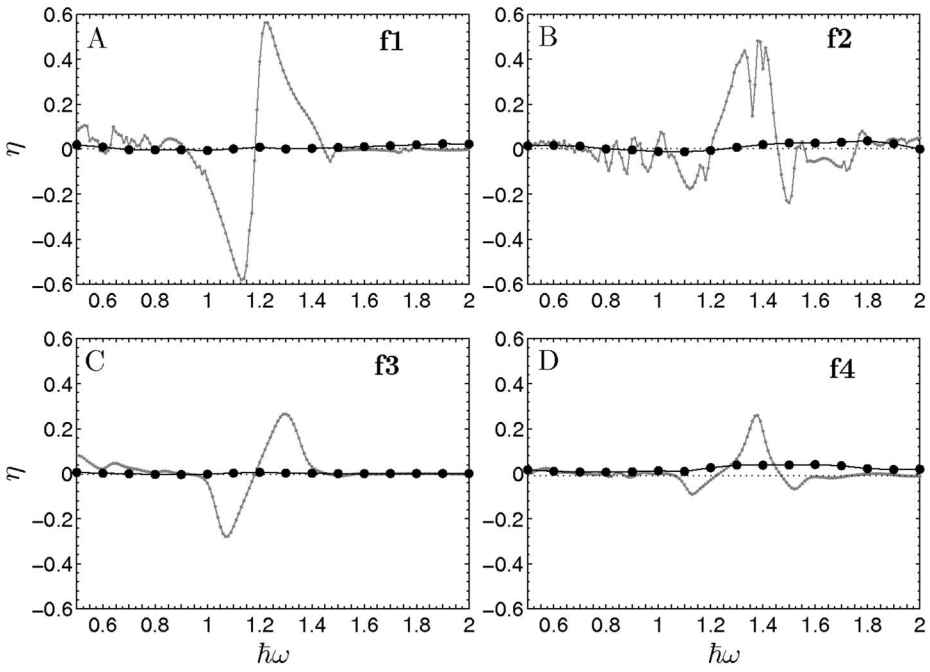


FIG. 4. Frequency dependence of the efficiency $\eta$ of the rectification generated by pulse: (A) f1, (B) f2, (C) f3, and (D) f4, with $\phi_{2\omega}-2\phi_{\omega}=0$. The black dots show the behavior of the flexible chain, while the gray lines correspond to the rigid case.

modifies the physical picture. As shown in Figs. 3 and 4, lattice fluctuations smear out the resonances observed in rigid wires resulting in control maps with broad features only. Although the scenario is successful in generating phase controllable currents (see, e.g., Fig. 5) with magnitudes that are often larger than the ones observed in rigid wires, the efficiency of the process is invariably very low irrespective of the driving frequency, laser intensity, or bandwidth (Fig. 4). That is, most photoexcited electrons do not participate of the currents and the enhancement of the effect is due to increased light absorption of the flexible wire relative to the rigid case. The highest observed efficiencies, obtained for moderately strong short pulses [Figs. 3 and 4(d)], are merely $\eta \approx 0.04$. These results clarify the previously unexplained origin for the enhancement of currents by increasing vibronic coupling strength observed in Ref. 30.

### B. Currents through the dynamic Stark effect

Thus far, our approach has been to excite electrons across the energy gap of the wire by tuning the frequencies of the field near a resonance of the system. We have seen, however, that this technique is fragile to decoherence processes since it relies on creating coherent superposition states. Lattice fluctuations make the rectification extremely inefficient and, in the best of cases, only about 4% of the electrons that are photoexcited participate in the net current. Hence, in order to induce sizable currents, considerable energy from the field must be dumped into the nanojunction, compromising its structural integrity. Further, employing faster or stronger pulses is not very helpful since they introduce other undesired satellite channels in the control and do not appreciably overcome the deleterious effects introduced by the vibrations.

In this section, we introduce an alternative mechanism that is remarkably robust to electron-vibrational couplings, survives in the presence of decoherence and thermal effects, and is able to induce large currents in molecular wires with efficiencies $>90\%$. Instead of promoting electrons to the conduction band through near-resonance photon absorption, we work far off resonance and employ Stark shifts to nonadiabatically couple the ground and excited electronic states. Phase-controllable symmetry breaking is achieved by exploiting the difference in the intensity of $\omega+2\omega$ fields for positive and negative amplitudes.

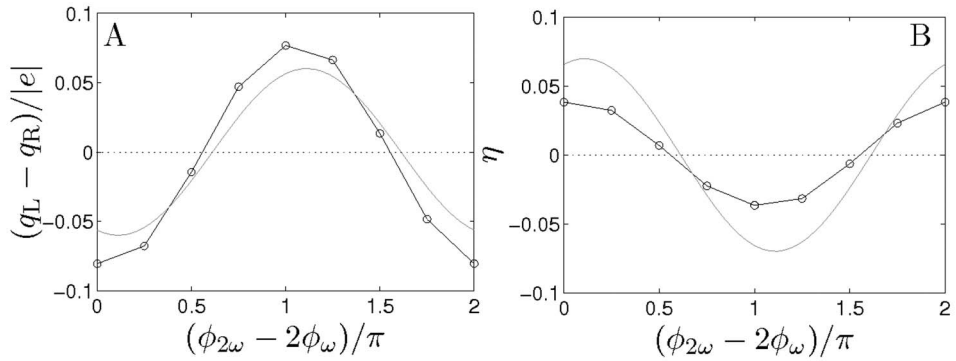


FIG. 5. Net transport as a function of the relative phase $\phi_{2\omega}-2\phi_{\omega}$ induced by pulse f4, with $\hbar\omega=1.3$ eV, in the rigid (gray lines) and the flexible (open circles) chains. Panel (A) shows the net difference in charge deposited; (B) depicts the efficiency of the process.

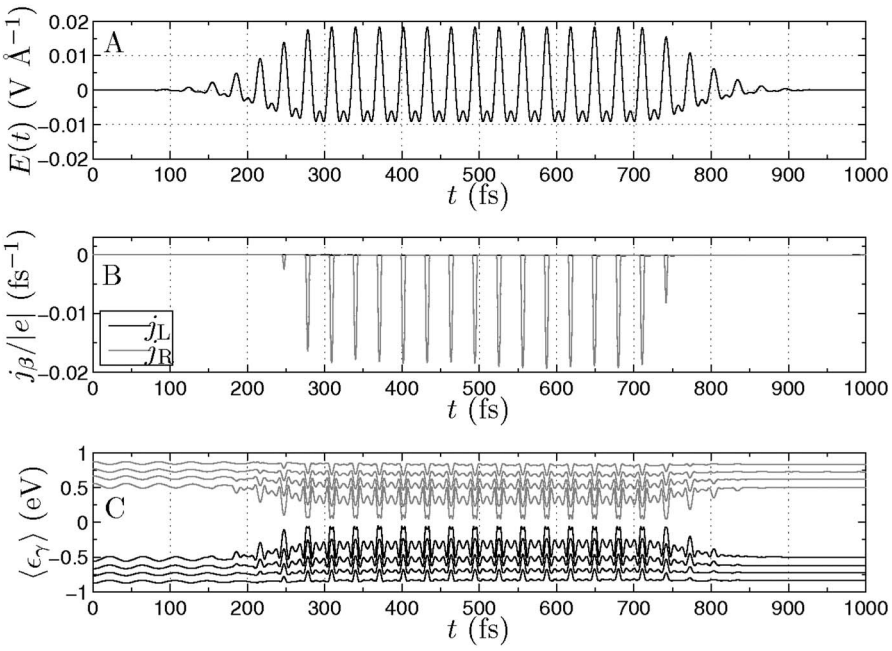


FIG. 6. Time dependence of (A) the electric field, (B) the current entering the left and right leads, and (C) the instantaneous light-dressed orbital energies for states near the energy gap for a 100 site flexible wire under the influence of the field in Eq. (39), with $\phi_{2\omega}-2\phi_\omega=0$. Note the bursts of charge deposited in the right lead when the field bridges the energy gap. Here, $j_L$ is so small that is barely visible.

Although this mechanism is applicable in medium sized chains ($N\approx 20$), it is best suited for long oligomers. Longer wires have a smaller energy gap, facilitating the coupling of ground and excited states through Stark shifts before photon absorption becomes dominant. For this reason, we consider perfectly dimerized neutral PA oligomers with $N=100$ sites ($L\approx 120.8$ Å) originally in the ground state configuration and propagate an ensemble of 1000 initial configurations. The electronic structure consists of $N/2$ doubly occupied $\pi$ (valence) orbitals and $N/2$ empty $\pi^\star$ (conduction band) states, separated by an energy gap of $2\Delta=1.3$ eV, which is significantly smaller than the 1.8 eV observed by 20 site oligomers. The average total energy of the ensemble is ~4.4 eV higher than its rigid counterpart due to zero-point fluctuations of the lattice in the ground electronic surface.

### 1. Complete control

We now illustrate the essentials of the phenomenon and show how under realistic conditions one can achieve almost complete control over the currents even in the presence of significant electron-phonon couplings. Consider the electron-vibrational dynamics of the wire under the influence of an $\omega+2\omega$ field of the form

$$E(t)=\sum_{n=1}^{2}\epsilon_{n\omega}\cos(n\omega t+\phi_{n\omega}) \times\begin{cases}\exp(-(t-t_{\rm on})^2/T_w^2) & \text{for } t\leqslant t_{\rm on}\\ 1 & \text{for } t_{\rm on}<t<t_{\rm off}\\ \exp(-(t-t_{\rm off})^2/T_w^2) & \text{for } t\geqslant t_{\rm off}.\end{cases} \quad (39)$$

The field is smoothly turned on and off in $T_w=100$ fs ($t_{\rm on}=300$ fs, $t_{\rm off}=700$ fs) and has constant amplitude for 400 fs. The frequency $\hbar\omega=0.2\Delta=0.13$ eV is chosen far off-resonance from the system's interband transition frequencies so that Stark shifts, and not photon absorption, dominate the dynamics. The field amplitude used is $\epsilon_{2\omega}=6.1\times10^{-3}$ V Å$^{-1}$ with $\epsilon_\omega=2\epsilon_{2\omega}$, which corresponds to an intensity $I_{2\omega}\sim 5\times10^8$ W cm$^{-2}$.

Figure 6 shows the field, the currents, and the light-dressed electronic structure of the flexible chain, averaged over all trajectories, when the relative phase of the pulse is $\phi_{2\omega}-2\phi_\omega=0$. Due to the highly polarizable nature of $\pi$-conjugated systems, the single-particle spectrum displays considerable Stark shifts, even at moderate field intensities, the effect being stronger for states near the edges of the valence and conduction band. In this way, the dynamic Stark effect effectively reduces the energy gap of the oligomer, causing frequent crossings between the ground and excited electronic states in individual trajectories. Since the wire's ground state is nondegenerate and of definite parity, the lowest-order contribution to the Stark effect is quadratic in the field. Hence, when $|E(t)|$ is maximum, the energy gap acquires its minimum value. At the crossing times, population is transferred from the valence to the conduction band and bursts of charge are deposited in the leads.

Note that for $\phi_{2\omega}-2\phi_\omega=0$, almost all excited electrons are deposited in the right contact only. Symmetry breaking arises due to the difference in the maximum $|E(t)|$ for positive and negative amplitudes exhibited by the field. Even when $E(t)$ has a zero temporal mean, it consists of narrow peaks with large $|E(t)|$ for positive amplitudes and shallow and broad features when $E(t)$ is negative [Fig. 6(a)]. For this reason, the Stark effect is only sufficiently strong to close the energy gap when the field has a positive amplitude. Thus, transfer of population to the conduction band and absorption of electrons by the leads always occur when the laser is pointing at a particular and the same direction, in this way inducing directed transport in the system.

The phenomenon depends intimately on the relative phase. For instance, for the case of $\phi_{2\omega}-2\phi_\omega=\pi/2$ shown in Fig. 7, the electric field exhibits equal intensity for positive and negative amplitudes. Since the field changes sign be-

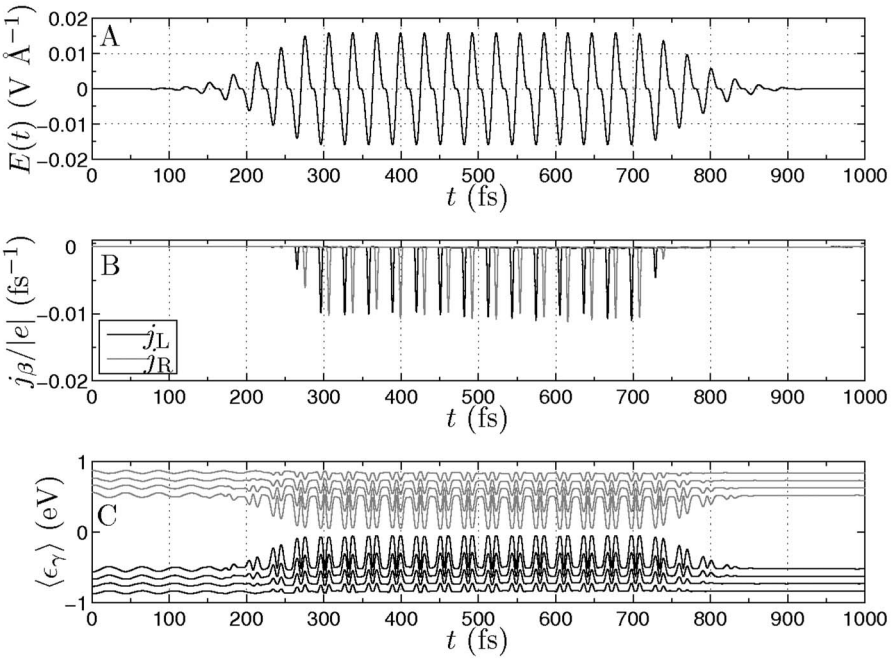


FIG. 7. Time dependence of (A) the electric field, (B) the current entering the left and right leads, and, (C) the instantaneous light-dressed orbital energies for states near the energy gap for a 100 site flexible wire under the influence of the field in Eq. (39), with $\phi_{2\omega}-2\phi_\omega=\pi/2$. Note that in this case, the bursts of charge deposited alternate between the left and right contacts.

tween consecutive interband couplings, the bursts of charge deposited alternate between the left and right contacts, and no net current is induced.

Figure 8 shows the net difference in charge deposited in the left and right leads after the pulse is over for different laser phases, as well as the efficiency of the process. For comparison purposes, the plot also includes results obtained in an equivalent but rigid system. We first note that the mechanism is robust to decoherence effects due to coupling to the vibrational degrees of freedom as well as satellite contributions due to parasite multiphoton absorption. In fact, 90% of the excited electrons can participate in the net current. This should be contrasted to the extremely low efficiencies achieved before through the multiphoton absorption mechanism. Further, the sign and magnitude of the effect can be manipulated by varying the laser phases. By changing the relative phase by $\pi$, the magnitude of the effect stays the same but the direction of the rectification is reversed.

In the flexible wire, the rectification exhibits an almost sinusoidal dependence on $\phi_{2\omega}-2\phi_\omega$. By contrast, in rigid wires for certain range of phases, no currents are induced since the maximum field amplitude is not large enough to couple valence and conduction bands. Hence, in this range, the currents observed in the flexible wire are phonon assisted; i.e., the level broadening introduced by the vibrations permits the nonadiabatic coupling. In fact, the currents observed in the flexible case are always larger than in the rigid example. However, in rigid wires, the mechanism can exhibit perfect efficiencies. The mechanism is also expected to be resilient to thermal effects. Increasing the temperature will introduce additional broadening of the electronic levels and, as pointed above, the Stark rectification is robust to this class of effects.

### 2. Possible satellite contributions

The simulations presented above exemplify how almost complete control over the electronic dynamics in the presence of vibronic couplings can be exerted in molecular wires. However, it is interesting to point out possible sources of satellite contributions that reduce the efficiency of this rectification mechanism. For definitiveness, consider the wire's dynamics under the influence of an $\omega+2\omega$ Gaussian pulse of the form

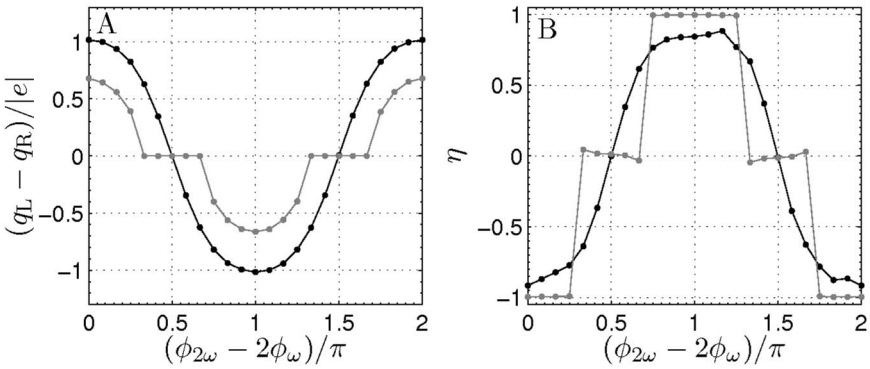


FIG. 8. Phase dependence of (A) the net rectification and (B) efficiency of the process when the field in Eq. (39) is applied to flexible and rigid 100 site PA wires (black dots, flexible wire; gray dots, rigid case). Note the assistance of phonons in the rectification.

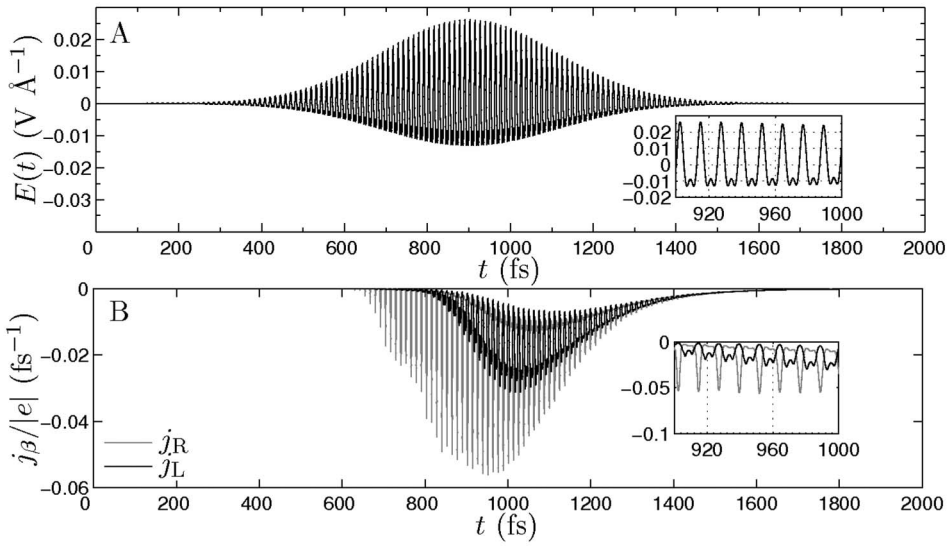


FIG. 9. Time dependence of (A) the electric field and (B) the current entering the left and right leads for a 100 site flexible wire under the influence of the field in Eq. (40), with $\phi_{2\omega}-2\phi_{\omega}=0$. The insets detail the field and currents from $t=900$ to 1000 fs.

$$E(t) = e^{-(t-T_c)^2/T_W^2} \sum_{n=1}^{2} \epsilon_{n\omega} \cos(n\omega t + \phi_{n\omega}), \tag{40}$$

centered at $T_c=900$ fs, with temporal width $T_W=300$ fs, and amplitudes $\epsilon_{2\omega}=8.7\times10^{-3}$ V Å$^{-1}$ with $\epsilon_{\omega}=2\epsilon_{2\omega}$, which corresponds to an intensity of $I_{2\omega}=10^9$ W cm$^{-2}$, and driving frequency $\hbar\omega=0.46\Delta=0.3$ eV. With respect to the field in Eq. (39), this laser profile has a higher maximum intensity and blueshifted central frequencies. Figure 9 shows the currents onset by this laser pulse when the relative phase is $\phi_{2\omega}-2\phi_{\omega}=0$, and Fig. 10 the total charge deposited during the dynamics. The field generates net currents along the system, with the right contact accepting 1.25 more electrons than the left one. However, in this case, only 9% of the excited electrons participate in the net current.

There are two sources of satellite contributions that reduce the efficiency of the scenario. The first is that some interband coupling occurs when the amplitude of the field is negative, contrary to the case described in the previous section. That is, the shallow negative amplitude of the field is sufficient to close the energy gap in some trajectories and deposit electrons in the left lead. Second, since the field frequency is larger than the one in Eq. (39), there is considerable excitation originating from photon absorption and not from Stark shifts. This leads to a background signal in $j_{\beta}(t)$ that does not contribute appreciably to the rectification and reduces the efficiency of the process. It is not difficult to suppress these two satellite effects by changing field parameters. Parasite multiphoton absorption can be avoided by further detuning the frequency of the field from the interband transition frequencies. Undesired closing of the energy gap can be circumvented by employing a laser profile with controlled and reduced intensity. Highly efficient current generation, such as that seen in the previous example, results.

## IV. CONCLUSIONS

Here, we have studied the possibility of inducing ultrafast currents using $\omega+2\omega$ fields along molecular wires with significant electron-vibrational couplings. Two possible mechanisms for laser-inducing rectification were identified. In the first one, electrons are excited across the energy gap of the wire by tuning the frequencies of the field near an electronic resonance of the system. By applying lasers with both $\omega$ and $2\omega$ components, asymmetry is generated in the momentum distribution of the photoexcited electrons. In the second mechanism, the $\omega+2\omega$ field is kept far off resonance and population is transferred to the excited states by means of Stark shifts that bridge the energy gap of the oligomer and, in this way, couple ground and excited electronic states. Symmetry breaking is achieved by exploiting the difference in the field's intensity for positive and negative amplitudes. This permits transferring population across the energy gap only when the field is pointing at a particular direction, thereby breaking the spatial symmetry of the system. In both cases, the magnitude and direction of the net currents are controllable by varying the relative phase of the two frequency components.

The vibronic couplings in the wire have very different effects in these two cases. In the first one, ultrafast decoher-

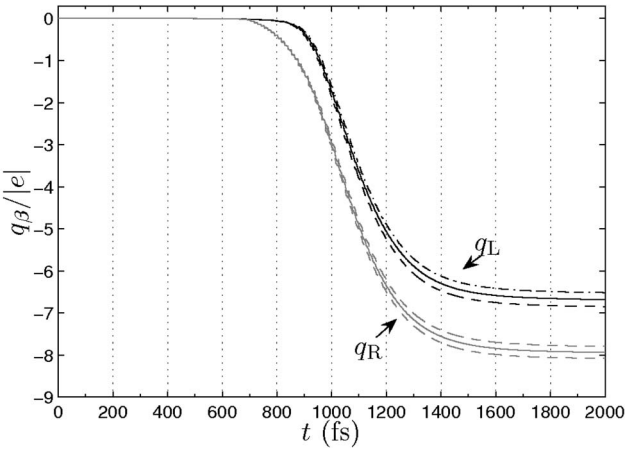


FIG. 10. Total charge deposited in the left $q_L$ (black line) and right $q_R$ (gray line) contacts during the dynamics of a 100 site flexible wire under the influence of the field in Eq. (40), with $\phi_{2\omega}-2\phi_{\omega}=0$. The dotted lines provide an estimate of the sampling errors.

ence processes induced by the wire's vibrations make the rectification effect extremely inefficient. While in rigid wires the maximum efficiency observed is ~60%, in flexible chains less than 4% of the photoexcited electrons participate in the current. This trend holds irrespective of the driving frequency, field strength, or width. At selected frequencies, the vibrations can enhance the magnitude of the effect, but not the efficiency, due to increased light absorption through level broadening. This observation sheds light on the previously unexplained observations reported in Ref. 30 where the magnitude of the photoinduced currents was shown to increase with the strength of the vibronic couplings. Note, however, that in order to generate sizable currents in this regime, a considerable number of electrons must be excited, undermining the structural stability of the system.

In contrast to the above mechanism, the off-resonance Stark mechanism introduced here is impervious to vibronic couplings. Even when the lattice dynamics may introduce parasite multiphoton absorption or undesired closing of the energy gap, these problems are easily overcome by redshifting the driving frequency and using pulses of lowered and controlled intensity. Simulations show that the mechanism can actually induce currents with efficiencies as high as 90%, in spite of the significant electron-phonon couplings.

We note that the actual implementation of these schemes poses substantial experimental challenges. The laser beam needs to be focused on the wire and the setup must control possible side effects that may arise from the illumination, such as heating, or processes involving excitation of the metal surface. Recent experimental developments[41–43] suggest that this may be possible. We hope that emerging applications, such as the one presented here, stimulate further experimental progress.

Lastly, from the simulations presented herein and a recent experiment[44], it is clear that the dynamic Stark effect is a promising tool to exert laser control that deserves further exploration. The success of this approach relies on the fact that it does not exploit the fragile properties of superposition states.


[1] S. M. Lindsay and M. A. Ratner, Adv. Mater. (Weinheim, Ger.) **19**, 23 (2007).
[2] A. Nitzan and M. A. Ratner, Science **300**, 1384 (2003).
[3] J. R. Heath and M. A. Ratner, Phys. Today **56**(5), 43 (2003).
[4] D. M. Adams, L. Brus, C. E. D. Chidsey, S. Creager, C. Creutz, C. R. Kagan, P. V. Kamat, M. Lieberman, S. Lindsay, R. A. Marcus, R. M. Metzger, M. E. Michel-Beyerle, J. R. Miller, M. D. Newton, D. R. Rolison, O. Sankey, K. S. Schanze, J. Yardley, and X. Y. Zhu, J. Phys. Chem. B **107**, 6668 (2003).
[5] A. Salomon, D. Cahen, S. Lindsay, J. Tomfohr, V. B. Engelkes, and C. D. Frisbie, Adv. Mater. (Weinheim, Ger.) **15**, 1881 (2003).
[6] C. Joachim and M. A. Ratner, Proc. Natl. Acad. Sci. U.S.A. **102**, 8801 (2005).
[7] A. Nitzan, Annu. Rev. Phys. Chem. **52**, 681 (2001).
[8] M. Shapiro and P. Brumer, *Principles of the Quantum Control of Molecular Processes* (Wiley, New York, 2003).
[9] I. Franco and P. Brumer, Phys. Rev. Lett. **97**, 040402 (2006).
[10] M. Cizek, M. Thoss, and W. Domcke, Phys. Rev. B **70**, 125406 (2004).
[11] E. G. Emberly and G. Kirczenow, Phys. Rev. B **61**, 5740 (2000).
[12] M. Galperin, M. A. Ratner, and A. Nitzan, J. Chem. Phys. **121**, 11965 (2004).
[13] M. Galperin, A. Nitzan, and M. A. Ratner, Phys. Rev. B **74**, 075326 (2006).
[14] V. May, Phys. Rev. B **66**, 245411 (2002).
[15] H. Ness and A. J. Fisher, Phys. Rev. Lett. **83**, 452 (1999).
[16] H. Ness, S. A. Shevlin, and A. J. Fisher, Phys. Rev. B **63**, 125422 (2001).
[17] A. Troisi, M. A. Ratner, and A. Nitzan, J. Chem. Phys. **118**, 6072 (2003).
[18] A. J. Heeger, Rev. Mod. Phys. **73**, 681 (2001).
[19] A. J. Heeger, S. Kivelson, J. R. Schrieffer, and W. P. Su, Rev. Mod. Phys. **60**, 781 (1988).
[20] I. Franco, M. Shapiro, and P. Brumer, J. Chem. Phys. **128**, 244905 (2008).
[21] D. Dulic, S. J. van der Molen, T. Kudernac, H. T. Jonkman, J. J. D. de Jong, T. N. Bowden, J. van Esch, B. L. Feringa, and B. J. van Wees, Phys. Rev. Lett. **91**, 207402 (2003).
[22] S. Yasutomi, T. Morita, Y. Imanishi, and S. Kimura, Science **304**, 1944 (2004).
[23] C. Zhang, M. H. Du, H. P. Cheng, X. G. Zhang, A. E. Roitberg, and J. L. Krause, Phys. Rev. Lett. **92**, 158301 (2004).
[24] A. Tikhonov, R. D. Coalson, and Y. Dahnovsky, J. Chem. Phys. **116**, 10909 (2002).
[25] A. Tikhonov, R. D. Coalson, and Y. Dahnovsky, J. Chem. Phys. **117**, 567 (2002).
[26] J. Lehmann, S. Kohler, and P. Hänggi, J. Chem. Phys. **118**, 3283 (2003).
[27] S. Welack, M. Schreiber, and U. Kleinekathofer, J. Chem. Phys. **124**, 044712 (2006).
[28] M. Galperin and A. Nitzan, Phys. Rev. Lett. **95**, 206802 (2005).
[29] M. Galperin and A. Nitzan, J. Chem. Phys. **124**, 234709 (2006).
[30] J. Lehmann, S. Kohler, V. May, and P. Hanggi, J. Chem. Phys. **121**, 2278 (2004).
[31] I. Franco, M. Shapiro, and P. Brumer, Phys. Rev. Lett. **99**, 126802 (2007).
[32] J. C. Tully, in *Classical and Quantum Dynamics in Condensed Phase Simulations*, edited by B. Berne, G. Ciccotti, and D. F. Coker (World Scientific, Singapore, 1998), pp. 700–720.
[33] L. L. Halcomb and D. J. Diestler, J. Chem. Phys. **84**, 3130 (1986).
[34] F. A. Bornemann, P. Nettesheim, and C. Schütte, J. Chem. Phys. **105**, 1074 (1996).
[35] O. V. Prezhdo and V. V. Kisil, Phys. Rev. A **56**, 162 (1997).
[36] M. Fox, *Optical Properties of Solids* (Oxford University Press, New York, 2001).
[37] J. R. Hellums and W. R. Frensley, Phys. Rev. B **49**, 2904 (1994).
[38] J. W. Negele and H. Orland, *Quantum Many Particle Systems* (Westview, Boulder, CO, 1998).
[39] *Handbook of Mathematical Functions*, edited by M. Abramowitz and I. A. Stegun (Dover, New York, 1965), Chap. 9.1.21.
[40] R. W. Brankin, I. Gladwell, and L. F. Shampine, *RKSUITE: A Suite of Runge-Kutta Codes for the Initial Value Problem for ODEs* (Softreport 92-S1, Department of Mathematics, Southern Methodist University, Dallas, Texas, 1992), www.netlib.org
[41] S. W. Wu, N. Ogawa, and W. Ho, Science **312**, 1362 (2006).
[42] L. Chen, J. Shakya, and M. Lipson, Opt. Lett. **31**, 2133 (2006).
[43] M. Aeschlimann, M. Bauer, D. Bayer, T. Brixner, F. J. Garcia de Abajo, W. Pfeiffer, M. Rohmer, C. Spindler, and F. Steeb, Nature (London) **446**, 301 (2007).
[44] B. J. Sussman, D. Townsend, M. Y. Ivanov, and A. Stolow, Science **314**, 278 (2006).